ISSN 1990-7931, Russian Journal of Physical Chemistry B, 2024, Vol. 18, No. 2, pp. 533–548. © The Author(s), 2024. This article is an open access publication, corrected publication 2024.

CHEMICAL PHYSICS OF ECOLOGICAL PROCESSES

Structural, Electromagnetic and Thermodynamic Analysis of Ion Pollutants Adsorption in Water by Gallium Nitride Nanomaterial: a Green Chemistry Application

F. Mollaamin[a], * and M. Monajjemi[b]

[a] *Department of Biomedical Engineering, Faculty of Engineering and Architecture, Kastamonu University, Kastamonu, Turkey*
[b] *Department of Chemical Engineering, Central Tehran Branch, Islamic Azad University, Tehran, Iran*
**e-mail: smollaamin@gmail.com*

Received October 26, 2023; revised December 8, 2023; accepted December 20, 2023

Abstract—Gallium nitride (Ga–N) nanocage can effectively remove alkali and alkaline earth metal ions from water. Therefore, it has been found a selective competition for metal cations in the Ga–N. The electronic, magnetic and thermodynamic properties of alkali-alkaline earth metal ion-adsorbed Ga–N have been investigated using density functional theory. The results denote that alkali/alkaline earth-metal ion-adsorbed Ga–N systems are stable compounds, with the most stable adsorption site being the center of the cage ring. In addition, because of charge transfer from Ga–N to the alkali/alkaline earth-metal cations show clear n-type adsorbing behavior. The absorption of alkali metal atoms on alkali/alkaline earth-metal cations occur via chemisorption. In this article, the behavior of trapping of main group cations of Li^+, Na^+, K^+, Be^{2+}, Mg^+ and Ca^{2+} by gallium nitride nanocone was observed for sensing the water metal cations. The essence of covalent traits for these clusters has displayed the similar energy value and image of the PDOS for the *p* states of N, the *d* states of Ga and *s* orbitals of metal cations including Li^+, Na^+, K^+/Be^{2+}, Mg^{2+} and Ca^{2+} through water treatment. The partial density of states (PDOS) can also estimate a certain charge assembly between Li^+, Na^+, K^+/Be^{2+}, Mg^{2+} and Ca^{2+} and Ga–N which indicate the complex dominant of metallic features and an exact degree of covalent traits between alkali/alkaline earth-metal cations and gallium nitride nanocage. Furthermore, the NMR spectroscopy has indicated the remarkable peaks around metal elements of Li^+, Na^+, K^+, Be^{2+}, Mg^+ and Ca^{2+} through the trapping in the Ga–N during ion detection and removal from water; however, there are some fluctuations in the chemical shielding behaviors of isotropic and anisotropy attributes. In addition, all accounted ΔG_R^o amounts are very close, which demonstrate the agreement of the measured specifications by all methodologies and the reliability of the computing values.

Keywords: water purification, nanomaterial, gallium nitride, metal ions
DOI: 10.1134/S199079312402012X

1. INTRODUCTION

The quality and quantity of the chemical elements in surface waters is affected by geo-chemical structure of surrounding area, land use, seasonal variations of weather conditions, vegetation and the atmospheric deposit [1–6].

The researchers have investigated the selectivity and priority of metal removal based on the type of surfactant in foam separation [7–9]. In general, according to Hoffmeister's series, it has been reported that alkali metals with smaller atomic numbers are more likely to precipitate with carboxylic acid in aqueous solutions [10–12]. The Hoffmeister's series was derived from the results of the protein salting-out effects ($Li^+ > Na^+ > K^+ > Rb^+ > Cs^+$). By contrast, micelles of surfactants with sulfate groups have a higher degree of binding of counterion with alkali metals of higher atomic numbers ($Li^+ < Na^+ < K^+ < Rb^+ < Cs^+$) [13].

The most common sources of ions that contribute to water hardness are from sedimentary rock (limestone and chalk) and soil runoff. Both calcium and magnesium are essential for human biology. Calcium increases bone mass and reduces the risk of fracture. Calcium deficiency can increase the chances of osteoporosis, hypertension, stroke, and various other cardiovascular issues. On the other hand, an excess of calcium can lead to hypercalcemia in those who are prone to milk alkali syndrome [14]. Magnesium is a cofactor for 350 cellular enzymes and is involved in protein and DNA/RNA synthesis. Magnesium deficiency can lead to hypertension, while excessive intake can have a laxative effect [15]. Although there are no

strict guidelines, hardness levels between 80 ppm and 100 ppm are recommended [16].

Furthermore, the results of chemical analysis show significant differences for the beryllium element concentration due to sampling season and sampling location [17].

Beryllium is not considered an essential element for humans and, in fact, is toxic and responsible for the chronic beryllium disease caused by beryllium exposure.

The GaN structure is one of the most discovered group III-nitride semiconductors which have been applied in different applications like electronic and optoelectronic devices, and sensor instruments [18–21]. Considering the prominent electronic properties of gallium nitride (GaN), it can be an appropriate case for gas sensing [22–28].

Compared with traditional semiconductor materials, three-dimensional GaN is a wide-band gap semiconductor material [29]. As such, it can enable equipment operation at ultra-high voltage, frequency, or temperature and exhibits high luminous efficiency, good thermal conductivity, high temperature resistance, resistance to acids and alkalis, and anti-radiation properties [30]. Atoms adsorbed onto a solid surface can interact indirectly through electron scattering or elastic distortion of the substrate, with the long-range atomic interaction modulated by the substrate playing an important role in atomic self-assembly. Because alkali-metal atoms can easily lose electrons, the adsorption of alkali metals onto semiconductor materials can change them to n-type, which will in turn reduce their work function and change their optoelectronic properties [31]. In recent years, many research groups have reported studies of the optoelectronic properties of alkali-metal-adsorbed 2D materials [32–42]. The adsorption of alkali-metal atoms on graphene [32, 33] and graphene-like gallium nitride (g-GaN) [43] using first-principles method was investigated and it was found that the optoelectronic properties of graphene and g-GaN) are modified by the adsorption of alkali-metal.

Adsorption involving charged adsorbates causes a change in the double layer and the potential at the outer Helmholtz plane, influencing the adsorption rates of both anodic and cathodic reactions. The first three modes are intimately with adsorption and the double layer the last involves interaction of the adsorbates molecules and the intermediate products formed during the partial electrochemical reactions, interaction of the adsorbed intermediates with organic molecules can either inhibit or enhance electrode reaction rate depending on the stability of the adsorbates-intermediate complex formed.

GaN alloy is relatively low in density and therefore, it is expected to extend the range of pollutants and overcome the inherited problems of poor adsorption, fast aggregation and secondary contamination in the remediation technology.

2. MATERIALS AND METHOD

2.1. Modelling of Atom-Trapping by Gallium Nitride

The intention of this work is removing some contaminants from the aqueous solution containing a group of alkali and alkaline earth metals. The model solution is composed of the target of an alkali/alkaline earth metal and the Ga–N in an aqueous solution (Fig. 1).

Gallium nitride nanocage was modeled in the presence of metal cations (Li^+, Na^+, K^+/Be^{2+}, Mg^{2+}, Ca^{2+}). Sample characterization was performed by CAM–B3LYP/EPR–3, LANL2DZ level of theory. The charge distribution of Li^+@Ga–N, Na^+@Ga–N, K^+@Ga–N, Be^{2+}@Ga–N, Mg^{2+}@Ga–N and Ca^{2+}@Ga–N complexes is calculated due to the Bader charge analysis [44].

The metal cations were successfully incorporated in the center of Ga–N towards formation of Li^+@Ga–N, Na^+@Ga–N, K^+@Ga–N, Be^{2+}@Ga–N, Mg^{2+}@Ga–N, and Ca^{2+}@Ga–N complexes (Fig. 1). Regardless of which metal, the Gallium nitride nanocage expanded to accommodate the metal ingredients.

2.2. Theoretical Computation by DFT/CAM-B3LYP

Considering the electronic density within the KS image directs us to a remarkable reduction of quantum computing. Thus, the KS methodology lightens the route for pursuing systems that cannot be discussed by conventional ab initio methodologies. Kohn and Sham introduces the solution which brings up the mono-electronic orbitals to account the kinetic energy in a simple and relatively exact, by finding a residual modification that might be computed apart [45, 46].

Therefore, the precise exchange energy functional is described by the Kohn–Sham orbitals in lieu of the density which is cited as the indirect density functional. This research has employed the penetration of the hybrid functional of three-parameter basis set of B3LYP (Becke, Lee, Yang, Parr) within the conception of density functional theory (DFT) upon theoretical computations [47, 48]. The B3LYP hybrid density functional is very prosperous in the investigation of thermochemistry of atoms and molecules for solids and surfaces and reproduces the experimental energy gaps and magnetic moments for a variety of materials [49].

First, the contribution of HF exchange was dampened to zero at short range, a feature that counteracts other advantages of hybrid functionals, leading Yanai and co-workers to suggest a variation, the Coulomb-attenuated B3LYP (CAM-B3LYP) method in which the damping function was empirically optimized to deliver robust performance for a wider range of molecular properties [50].

The first relevant implementation of CAM-B3LYP into a code for materials-science modelling has just been reported, an implementation into the Car-Parri-

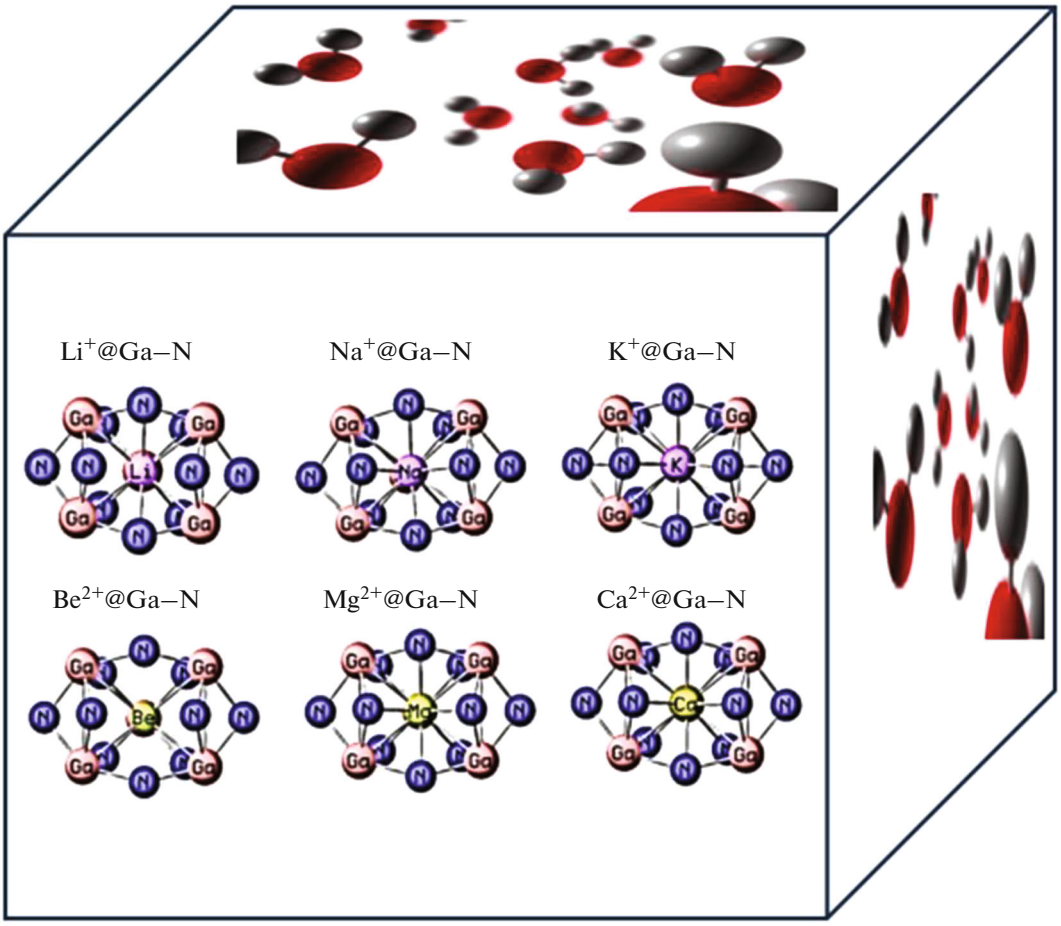

Fig. 1. The mechanism of encapsulation of the metal cations (Li^+, Na^+, K^+/Be^{2+}, Mg^{2+}, Ca^{2+}) in water by the gallium nitride nanocage and formation of Li^+@Ga–N, Na^+@Ga–N, K^+@Ga–N, Be^{2+}@Ga–N, Mg^{2+}@Ga–N and Ca^{2+}@Ga–N complexes.

nello molecule dynamic (CPMD) package for gamma-point-only calculations. The results obtained demonstrated enhanced optical spectra prediction, as expected [51].

In this article, the DFT calculations have been accomplished by using Gaussian 16 revision C.01 program package [52]. The input Z-matrix for encapsulation of the metal cations (Li^+, Na^+, K^+/Be^{2+}, Mg^{2+}, Ca^{2+}) in water by the gallium nitride nanocage has been provided with GaussView 6.1 [53] due to the rigid system and coordination format of which a blank line has been cited and using LANL2DZ basis set to distinguish chemical shielding, frequencies, thermodynamic properties, electrostatic and electronic potential, natural atomic charges, projected density of state and other quantum properties for this work.

3. RESULTS AND DISCUSSION

In this article, the data has evaluated the efficiency of gallium nitride (Ga–N) nanocage for metal cations encapsulation. In fact, it can be remarked the chemisorptive nature of the bond among the metal cations with gallium and nitrogen elements through the equilibrium distribution of metal cations, Ga–N, and a monolayer behavior.

3.1. Density of States Analysis

The electronic structures of (Li^+, Na^+, K^+/Be^{2+}, Mg^{2+}, Ca^{2+})–trapped Ga–N as the selective sensor for detecting and grabbing the metal cations in water have been investigated to simplify subsequent study for interfacial electronic properties using CAM–B3LYP/EPR–3, LANL2DZ level of theory.

Figures 2a–2f shows the projected density of state (PDOS) of (Li^+, Na^+, K^+/Be^{2+}, Mg^{2+}, Ca^{2+})–trapped Ga–N through metal cation adsorption. The appearance of the energy states (*s*-orbital) of Li^+, Na^+, K^+/Be^{2+}, Mg^{2+}, Ca^{2+} within the gap of Ga–N induces the reactivity of the system. It is clear from the figure that after trapping with metal cations, there is a significant contribution of metal cations *s*-orbital in the unoccupied level. Based on the population analysis

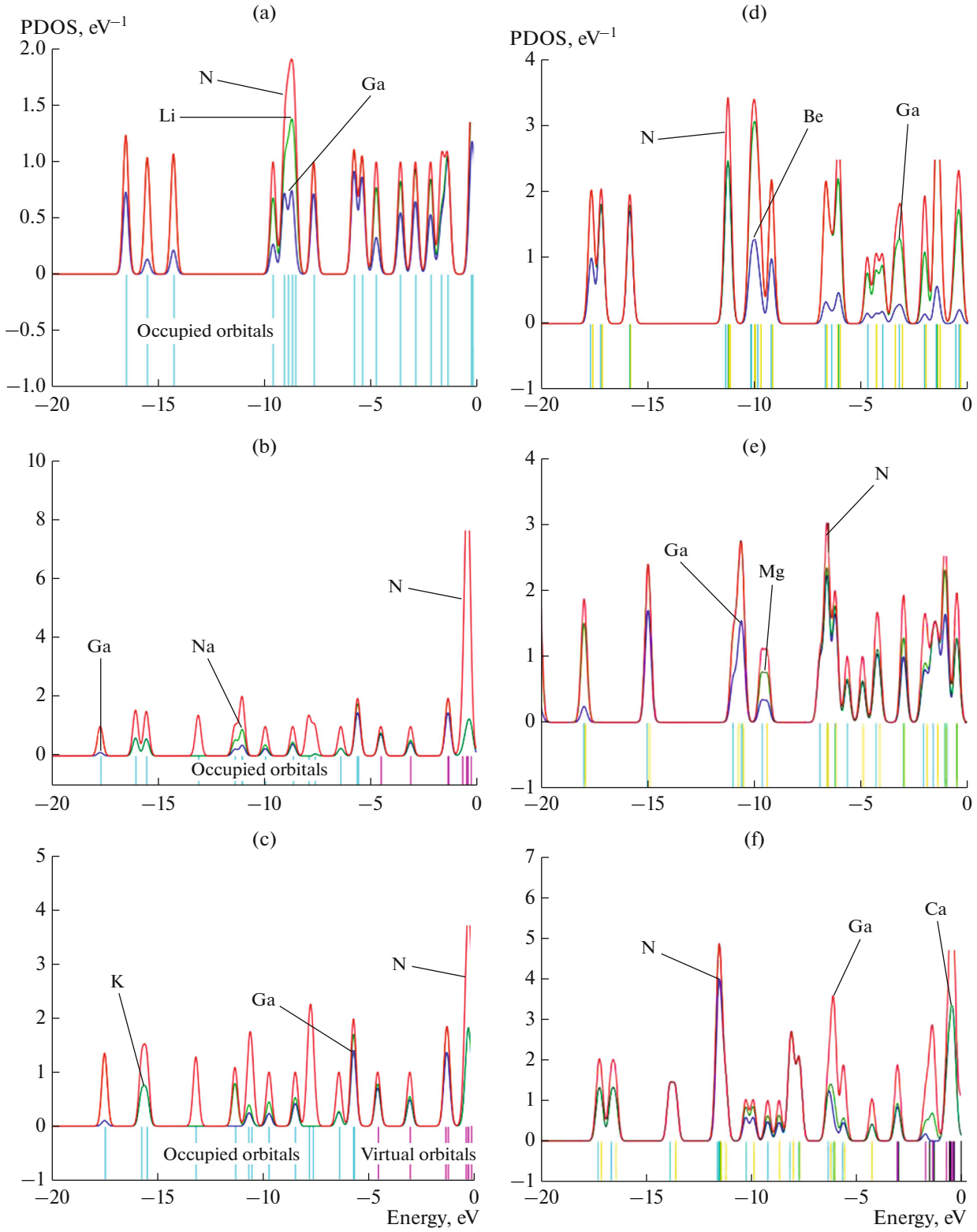

Fig. 2. PDOS of (a) Li^{+}@Ga–N, (b) Na^{+}@Ga–N, (c) K^{+}@Ga–N, (d) Be^{2+}@Ga–N, (e) Mg^{2+}@Ga–N, and (f) Ca^{2+}@Ga–N complexes by CAM–B3LYP/EPR–3, LANL2DZ.

Table 1. The electric potential (a.u.) and Bader charge (e) through NQR calculation for Li^+@Ga–N, Na^+@Ga–N, K^+@Ga–N, Be^{2+}@Ga–N, Mg^{2+}@Ga–N, and Ca^{2+}@Ga–N complexes using CAM-B3LYP/EPR–3, LANL2DZ calculation

Atom	Q	E_p	Atom	Q	E_p	Atom	Q	E_p
Li^+@Ga–N			Na^+@Ga–N			K^+@Ga–N		
Ga1	0.92	−146.60	Ga1	0.88	−146.60	Ga1	0.87	−146.57
N2	−0.2	−18.14	N2	−0.48	−18.16	N2	−0.46	−18.17
N3	−0.46	−18.15	N3	−0.51	−18.17	N3	−0.53	−18.18
Ga4	0.90	−146.60	Ga4	0.88	−146.60	Ga4	0.83	−146.57
Ga5	0.90	−146.61	Ga5	0.86	−146.62	Ga5	0.87	−146.61
Ga6	0.92	−146.62	Ga6	0.88	−146.63	Ga6	0.89	−146.60
N7	−0.41	−18.14	N7	−0.46	−18.15	N7	−0.44	−18.16
N8	−0.46	−18.15	N8	−0.51	−18.17	N8	−0.53	−18.17
N9	−0.45	−18.17	N9	−0.49	−18.18	N9	−0.51	−18.19
N10	−0.45	−18.16	N10	−0.49	−18.17	N10	−0.50	−18.18
N11	−0.44	−18.16	N11	−0.47	−18.17	N11	−0.48	−18.18
N12	−0.50	−18.17	N12	−0.54	−18.19	N12	−0.57	−18.20
Ga13	0.5	−146.61	Ga13	0.93	−46.61	Ga13	0.86	−146.62
N14	−0.44	−18.13	N14	−0.45	−18.13	N14	−0.45	−18.13
N15	−0.44	−18.13	N15	−0.44	−18.13	N15	−0.44	−18.12
Li16	−0.11	−5.59	Na16	0.42	−34.52	K16	0.60	−74.29
Be^{2+}@Ga–N			Mg^{2+}@Ga–N			Ca^{2+}@Ga–N		
Ga1	0.98	−146.59	Ga1	0.88	−146.58	Ga1	0.85	−146.57
N2	−0.47	−18.18	N2	−0.50	−18.17	N2	−0.49	−18.16
N3	−0.46	−18.16	N3	−0.53	−18.18	N3	−0.59	−18.19
Ga4	0.97	−146.58	Ga4	0.89	−146.58	Ga4	0.84	−146.57
Ga5	0.96	−146.58	Ga5	0.86	−146.60	Ga5	0.84	−146.56
Ga6	0.98	−146.59	Ga6	0.89	−146.58	Ga6	0.87	−146.58
N7	−0.45	−18.17	N7	−0.49	−18.17	N7	−0.46	−18.15
N8	−0.47	−18.16	N8	−0.55	−18.18	N8	−0.62	−18.20
N9	−0.44	−18.17	N9	−0.52	−18.18	N9	−0.55	−18.19
N10	−0.45	−18.17	N10	−0.52	−18.18	N10	−0.55	−18.20
N11	−0.43	−18.16	N11	−0.50	−18.18	N11	−0.53	−18.18
N12	−0.49	−18.16	N12	−0.57	−18.18	N12	−0.64	−18.21
Ga13	1.07	−146.59	Ga13	0.97	−146.60	Ga13	0.82	−146.61
N14	−0.49	−18.18	N14	−0.46	−18.14	N14	−0.45	−18.13
N15	−0.46	−18.15	N15	−0.45	−18.15	N15	−0.44	−18.12
Be16	−0.34	−8.28	Mg16	0.62	−38.93	Ca16	1.10	−79.46

and DOS (density of state), it can be concluded that metal cations remain in the cationic state, and it can accept more electrons from other atoms. Therefore, the curve of partial DOS/PDOS has described that the *p* states of N atoms and *d* states of Ga atoms in Ga–N overcome due to the conduction band (Figs. 2a–2f). A distinguished metallic trait might be seen in MCs@Ga–N because of the potent interaction between the *p* states of N, the *d* states of Ga and the s states of Li^+, Na^+, K^+/Be^{2+}, Mg^{2+}, Ca^{2+} near the Fermi energy. Furthermore, the essence of covalent traits for these clusters has displayed the similar energy value and image of the PDOS for the *p* states of N, the *d* states of Ga and *s* orbitals of metal cations including Li^+, Na^+, K^+/Be^{2+}, Mg^{2+} and Ca^{2+} through water treatment (Figs. 2a–2f).

Figures 2a–2f shows that Li^+@Ga–N, Na^+@Ga–N, K^+@Ga–N, Be^{2+}@Ga–N, Mg^{2+}@Ga–N, and Ca^{2+}@Ga–N complexes through metal cation

adsorption, respectively, have the most contribution at the middle of the conduction band between −5 to −10 eV, while contribution of gallium and nitrogen states are enlarged and similar together, and encapsulating of Li^+, Na^+, K^+/Be^{2+}, Mg^{2+} and Ca^{2+} depicts interfacial electronic of the Ga–N for selection of these cations.

3.2. Electrostatic Properties Evaluation

As the electric field gradient (EFG) at the citation of the nucleus in metal cations including Li^+, Na^+, K^+/Be^{2+}, Mg^{2+} and Ca^{2+} is allocated by the valence electrons twisted in the particular attachment with close nuclei of Ga–N through trapping of metal cations, the nuclear quadrupole resonance (NQR) frequency at which atoms occur is particular for M@Ga–N complexes (M = Li^+, Na^+, K^+/Be^{2+}, Mg^{2+}, Ca^{2+}) (Table 1). NQR is a straight frame of the interaction of the quadrupole moment with the EFG which is produced by the electronic structure of its ambiance. Therefore, the NQR atom frequencies are symmetric to the electric quadrupole moment of the nucleus and a measurement of the strength of the local EFG [54–57].

In this research work, the electric potential as the quantity of work energy through carrying over the electric charge from one position to another position in the essence of electric field has been evaluated for Li^+@Ga–N, Na^+@Ga–N, K^+@Ga–N, Be^{2+}@Ga–N, Mg^{2+}@Ga–N, and Ca^{2+}@Ga–N complexes using CAM–B3LYP/EPR–3,LANL2DZ level of theory (Table 1).

Furthermore, in Figs. 3a–3f, it has been sketched the electric potential of nuclear quadrupole resonance for some atoms of (Li^+, Na^+, K^+/Be^{2+}, Mg^{2+}, Ca^{2+}) in the trapping in the Ga–N through metal cations adsorption which has been calculated by CAM–B3LYP/EPR–3, LANL2DZ. In Figs. 3a–3f, it was observed the behavior of trapping of main group cations of Li^+, Na^+, K^+, Be^{2+}, Mg^+ and Ca^{2+} by gallium nitride nanocone for sensing the water metal cations. It's vivid that the curve of Ga–N is waved by these metal cations. The sharpest peaks for electric potential have been shown around metal cations trapping on the Ga–N which present the electron accepting characteristics of these atoms versus the gallium and nitrogen atoms of Ga–N.

3.3. Analysis of Electromagnetic Specifications

From the DFT calculations, it has been attained the chemical shielding (CS) tensors in the principal axes system to estimate the isotropic chemical-shielding (CSI) and anisotropic chemical-shielding (CSA) [58]:

$$\sigma_{iso} = (\sigma_{11} + \sigma_{22} + \sigma_{33})/3, \quad (1)$$

$$\sigma_{aniso} = \sigma_{33} - \frac{\sigma_{22} + \sigma_{11}}{2}. \quad (2)$$

The chemical shielding extracts from NMR can be applied for allocating the structural and geometrical specifications of materials. As a matter of fact, gauge invariant atomic orbital (GIAO) methodology has been recommended as a valid methodology for NMR parameter computations and Our own N-layered integrated molecular irbital and molecular mechanics (ONIOM) has caught many regards for gaining NMR chemical shielding of gas molecule-surface complexes such as isotropic chemical shielding appears in Eq. (3):

$$\sigma_{iso,\ ONIOM} = \sigma_{iso,\ high(QM1)} + \sigma_{iso,\ medium(QM2)} + \sigma_{iso,\ low(QM3)}. \quad (3)$$

The NMR data of isotropic (σ_{iso}) and anisotropic shielding tensor (σ_{aniso}) of Li^+, Na^+, K^+, Be^{2+}, Mg^+ and Ca^{2+} trapped on the in the Ga–N towards formation of Li^+@Ga–N, Na^+@Ga–N, K^+@Ga–N, Be^{2+}@Ga–N, Mg^{2+}@Ga–N, and Ca^{2+}@Ga–N complexes have been computed by Gaussian 16 revision C.01 program package [52] and been shown in Table 2.

In Table 2, NMR data has reported the notable amounts for metal cations of Li^+, Na^+, K^+, Be^{2+}, Mg^+ and Ca^{2+}which were trapped in the Ga–N as the selective sensor for detecting metal ions in water. In fact, the encapsulation of Li^+, Na^+, K^+, Be^{2+}, Mg^+ and Ca^{2+} ions can introduce spin polarization on the MCs (Li^+, Na^+, K^+, Be^{2+}, Mg^+ and Ca^{2+})–encapsulated Ga–N which indicates that these surfaces might be applied as the magnetic energy storage. In fact, it is revealed that the isotropic and anisotropic shielding fluctuate with the occupancy in the electron accepting metal cations trapped in the gallium nitride nanocage.

Figures 4a–4f exhibited the same tendency of shielding for magnesium and aluminum; however a considerable deviation from metal cations of lithium (Fig. 4a), sodium (Fig. 4b), potassium (Fig. 4c), beryllium (Fig. 4d), magnesium (Fig. 4e), and calcium (Fig. 4f) through trapping in the gallium nitride nanocage. In Figs. 4a–4f, metal atoms of Li^+, Na^+, K^+, Be^{2+}, Mg^+ and Ca^{2+} in the complexes of Li^+@Ga–N (Fig. 4a), Na^+@Ga–N (Fig. 4b), K^+@Ga–N (Fig. 4c), Be^{2+}@Ga–N (Fig. 4d), Mg^{2+}@Ga–N (Fig. 4e), and Ca^{2+}@Ga–N (Fig. 4f) denote the fluctuation in the chemical shielding during ion trapping.

In fact, Figs. 4a–4f indicates that the gap chemical shielding between gallium/nitrogen in Ga–N nanocage and metal cations. Therefore, it can be considered that the efficiency of electron accepting for the trapped metal cations in the Ga–N is $Ca^{2+} \approx K^+ > Mg^{2+} \approx Na^+ > Be^{2+} \approx Li^+$ that indicate the power of covalent bond between gallium/nitrogen and these metal cations towards ion removal.

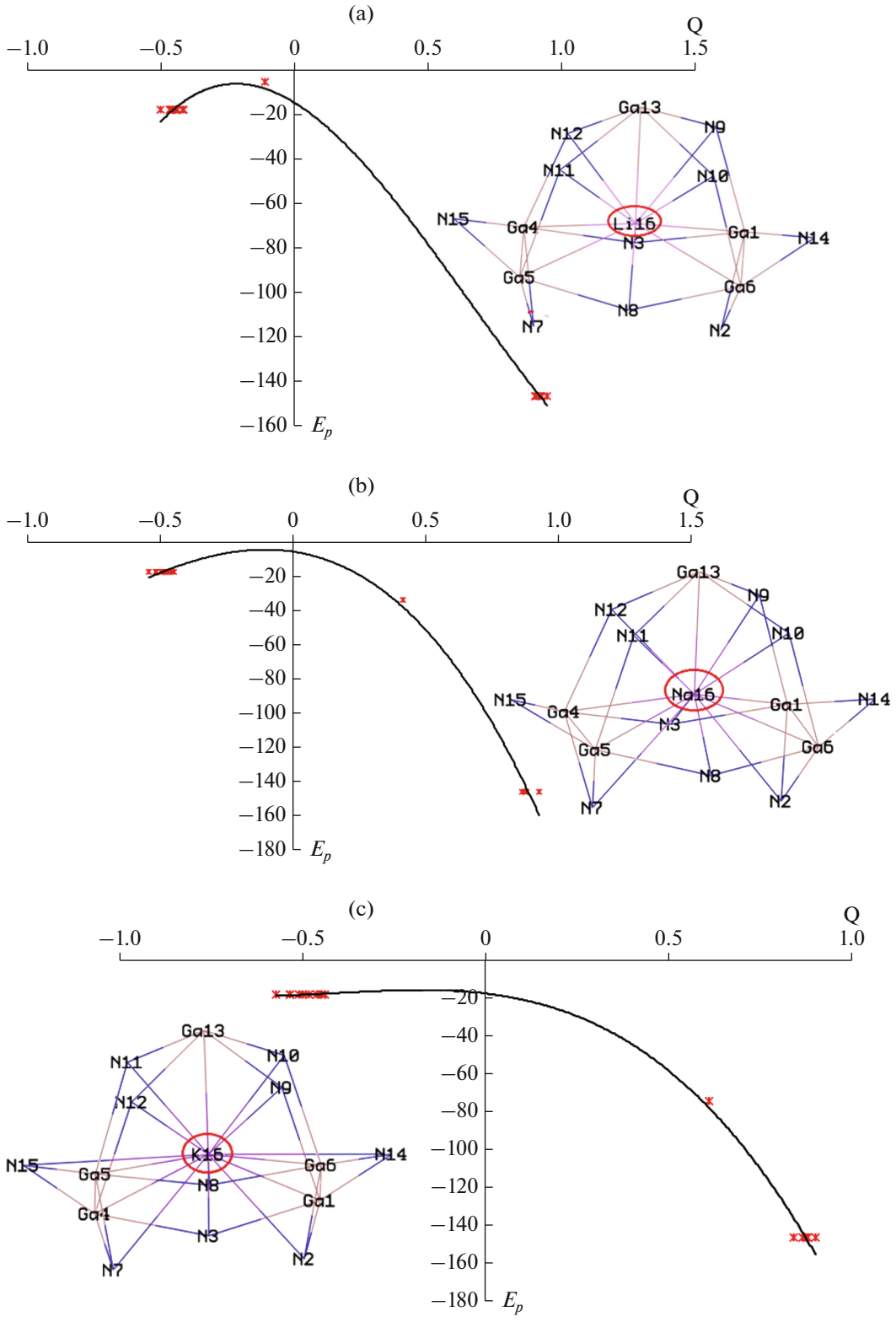

Fig. 3. Electric potential (a.u.) versus Bader charge (e) through NQR calculation for (a) Li^{+}@Ga–N, (b) Na^{+}@Ga–N, (c) K^{+}@Ga–N, (d) Be^{2+}@Ga–N, (e) Mg^{2+}@Ga–N, and (f) Ca^{2+}@Ga–N complexes by CAM–B3LYP/EPR–3, LANL2DZ.

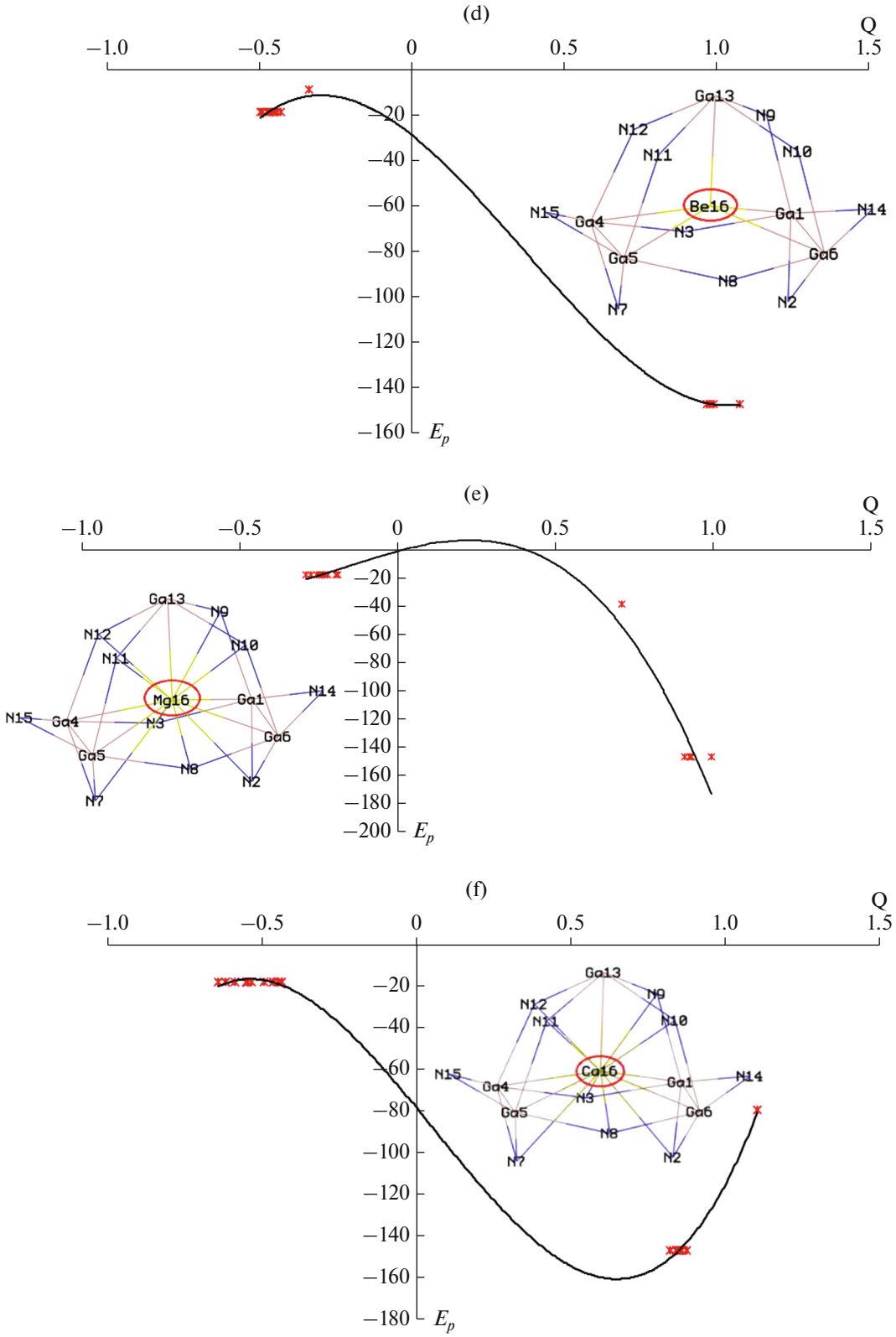
(d)
Q
−1.0
−0.5
0
0.5
1.0
1.5
−20
−40
−60
−80
−100
−120
−140
−160
E_p
Ga13
N9
N12
N11
N10
Be16
N15
Ga4
Ga1
N14
N3
Ga5
Ga6
N8
N7
N2
(e)
Q
−1.0
−0.5
0
0.5
1.0
1.5
−20
−40
−60
−80
−100
−120
−140
−160
−180
−200
E_p
Ga13
N9
N12
N11
N10
Mg16
Ga1
N14
N15
Ga4
N3
Ga6
Ga5
N8
N2
N7
(f)
Q
−1.0
−0.5
0
0.5
1.0
1.5
−20
−40
−60
−80
−100
−120
−140
−160
−180
E_p
Ga13
N9
N12
N11
N10
Ca16
N15
Ga4
Ga1
N14
N3
Ga5
Ga6
N8
N7
N2

Fig. 3. (Contd.)

Table 2. Data of NMR shielding tensors for selected atoms of Li^+@Ga–N, Na^+@Ga–N,K^+@Ga–N, Be^{2+}@Ga–N, Mg^{2+}@Ga–N, and Ca^{2+}@Ga–N complexes using CAM-B3LYP/LANL2DZ calculation

Atom	σ_{iso}	σ_{aniso}	Atom	σ_{iso}	σ_{aniso}	Atom	σ_{iso}	σ_{aniso}
Li^+@Ga–N			Na^+@Ga–N			K^+@Ga–N		
Ga1	94.43	3066.61	Ga1	176.04	3288.77	Ga1	176.04	3288.77
N2	186.79	1011.44	N2	146.21	962.64	N2	146.21	962.64
N3	629.68	1767.88	N3	559.40	1683.75	N3	559.40	1683.75
Ga4	196.55	3474.46	Ga4	313.19	3636.45	Ga4	313.19	3636.45
Ga5	734.39	3510.34	Ga5	664.68	3206.29	Ga5	664.68	3206.29
Ga6	542.09	3175.75	Ga6	426.04	2698.25	Ga6	426.04	2698.25
N7	95.19	707.84	N7	81.15	707.77	N7	81.15	707.77
N8	68.18	588.37	N8	317.19	1085.01	N8	317.19	1085.01
N9	150.08	746.45	N9	190.49	825.50	N9	190.49	825.50
N10	293.94	1194.23	N10	212.97	1100.90	N10	212.97	1100.89
N11	340.28	1177.34	N11	183.17	944.69	N11	183.17	944.69
N12	12.10	577.10	N12	41.68	684.34	N12	41.68	684.34
Ga13	27.34	1481.09	Ga13	48.80	1547.57	Ga13	48.80	1547.57
N14	312.46	578.11	N14	307.12	507.19	N14	307.12	507.19
N15	354.60	765.44	N15	339.25	700.61	N15	339.25	700.61
Li16	97.29	38.06	Na16	489.74	66.83	K16	489.74	66.83
Be^{2+}@Ga–N			Mg^{2+}@Ga–N			Ca^{2+}@Ga–N		
Ga1	64.76	2402.33	Ga1	11.39	2416.36	Ga1	250.22	2403.78
N2	21.01	462.56	N2	62.56	393.01	N2	62.07	442.92
N3	21.81	425.95	N3	45.58	575.36	N3	101.18	610.93
Ga4	151.67	2670.64	Ga4	193.87	2550.73	Ga4	144.77	2714.41
Ga5	217.96	2534.48	Ga5	90.09	2280.16	Ga5	43.85	2502.24
Ga6	115.91	1848.10	Ga6	81.79	2253.42	Ga6	344.25	2242.45
N7	38.23	600.30	N7	88.81	478.94	N7	61.26	467.03
N8	37.65	416.07	N8	19.86	479.76	N8	90.78	544.82
N9	14.56	306.71	N9	6.18	350.23	N9	75.20	372.25
N10	50.57	466.05	N10	68.52	453.77	N10	161.00	524.31
N11	83.01	534.34	N11	96.98	466.54	N11	135.69	565.42
N12	130.08	314.72	N12	80.72	328.60	N12	62.56	493.85
Ga13	239.36	1231/00	Ga13	287.15	1368.73	Ga13	357.74	1443.34
N14	42.01	340.40	N14	173.30	239.35	N14	198.07	130.56
N15	181.45	267.58	N15	134.01	299.82	N15	208.97	246.76
Be16	133.40	14.64	Mg16	614.43	39.29	Ca16	1130.04	118.07

3.4. Thermochemistry Computations

Infrared (IR) calculations have been accomplished for trapping of metal cations of Li^+, Na^+, K^+, Be^{2+}, Mg^+ and Ca^{2+} in the Ga–N during ion sensing in water. Therefore, it has been simulated the several clusters containing Li^+@Ga–N (Fig. 5a), Na^+@Ga–N (Fig. 5b), K^+@Ga–N (Fig. 5c), Be^{2+}@Ga–N (Fig. 5d), Mg^{2+}@Ga–N (Fig. 5e), and Ca^{2+}@Ga–N (Fig. 5f). The graph of Fig. 5a has been observed in the frequency range between 100–1150 cm^{-1} for Li^+@Ga–N with a several sharp peaks around 380.73, 751.19, 760.13 and 1069.76 cm^{-1}. Figure 5b has shown the frequency range between 100–1150 cm^{-1} for Na^+@Ga–N with sharp peaks around 281.61, 360.46, and 891.95 cm^{-1}. Figure 5c has indicated the fluctuation of frequency between 100–1400 cm^{-1} for K^+@Ga–N with two sharp peaks around 511.8 and 1257.49 cm^{-1}. Figure 5d has shown the fluctuation of frequency

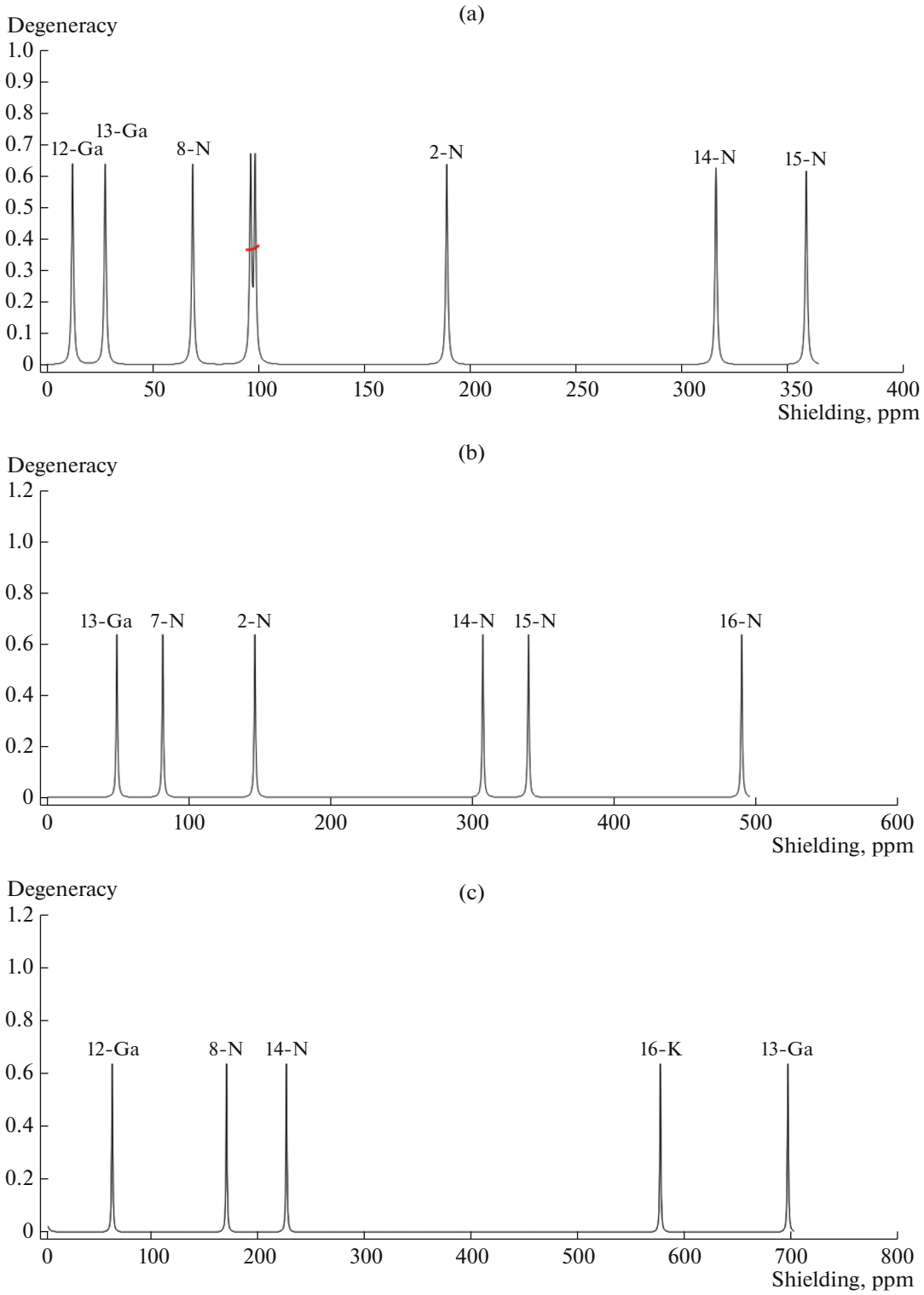

Fig. 4. The NMR spectra for (a) Li^{+}@Ga–N, (b) Na^{+}@Ga–N, (c) K^{+}@Ga–N, (d) Be^{2+}@Ga–N, (e) Mg^{2+}@Ga–N, and (f) Ca^{2+}@Ga–N complexes using CAM-B3LYP/LANL2DZ.

between 100–900 cm^{-1} for Be^{2+}@Ga–N with a few sharp peaks around 198.48, 294.64, 332.54, 496.22, 848.60 and 870.73 cm^{-1}. Moreover, it has been observed the frequency between 150–900 for Mg^{2+}@Ga–N with sharp peaks around 147.30, 411.29, 419.59, 448.44, and 464.69 cm^{-1} (Fig. 5e). Besides,

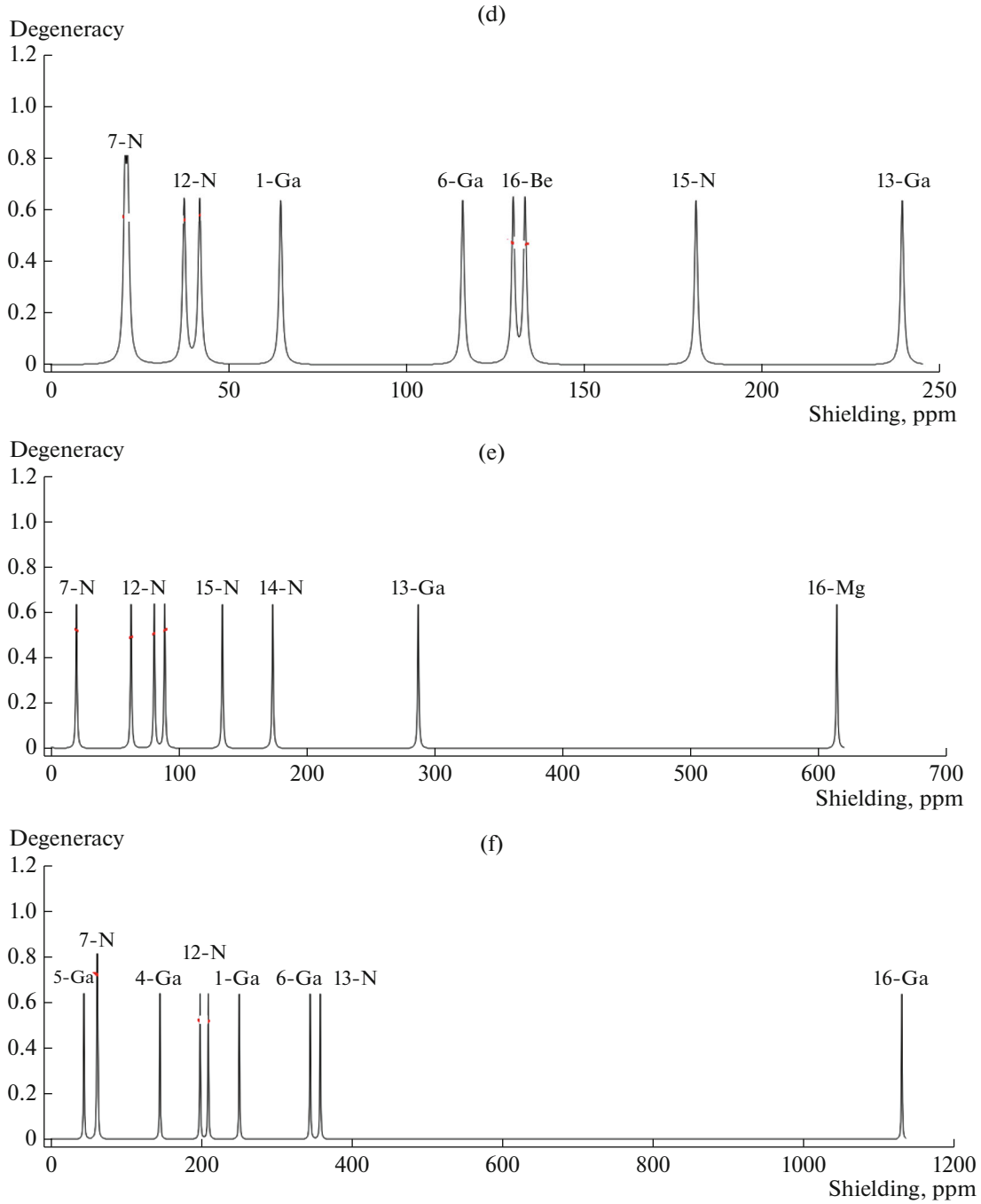

Fig. 4. (Contd.)

Fig. 5f has exhibited the frequency between 150–1400 for Ca^{2+}@Ga–N with sharp peaks around 561.35, 629.19, 630.22, 661.03, and 669.48 cm^{-1}.

Table 3 through the thermodynamic specifications concluded that Ga–N due to encapsulation of metal cations including Li^+, Na^+, K^+, Be^{2+}, Mg^+ and Ca^{2+} might be more efficient sensor for detecting and removing the metal cations from water. The thermodynamic data in Table 3 could detect the maximum efficiency of metal cations (Li^+, Na^+, K^+, Be^{2+}, Mg^+ and Ca^{2+}) trapped in the Ga–N through ΔG_R^o which depends on the covalent bond between first and second main group metal cations and Ga–N as a potent sensor for water treatment.

The encapsulation process of metal cations (Li^+, Na^+, K^+, Be^{2+}, Mg^+ and Ca^{2+}) in Ga–N is affirmed by the ΔG_f^o quantities:

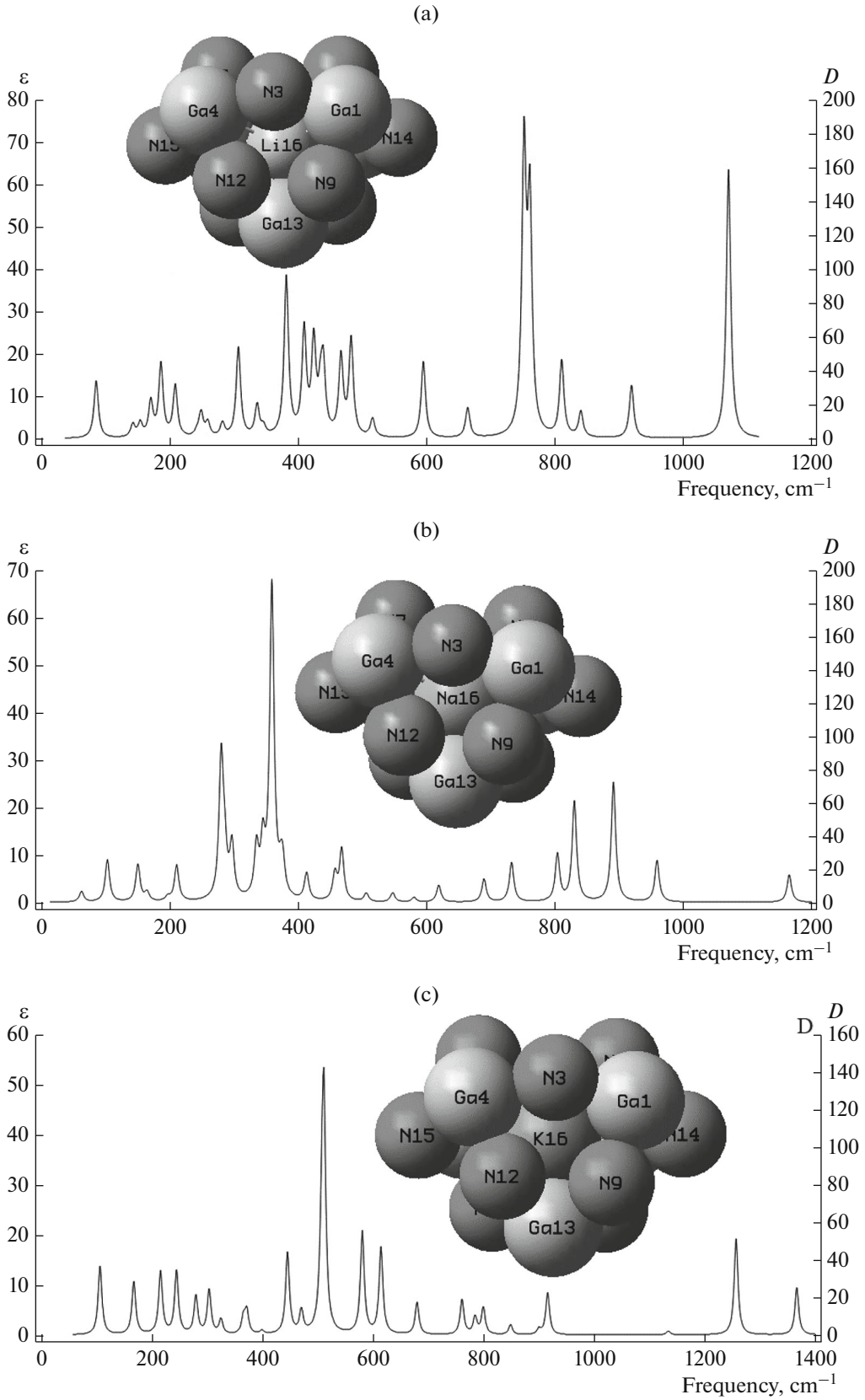

Fig. 5. The frequency (cm^{-1}) changes through the IR spectra for (a) Li^{+}@Ga–N, (b) Na^{+}@Ga–N, (c) K^{+}@Ga–N, (d) Be^{2+}@Ga–N, (e) Mg^{2+}@Ga–N, and (f) Ca^{2+}@Ga–N complexes (Note: ε (M^{-1} cm^{-1} or L mol^{-1} cm^{-1}) is the absorbance unit and D (10^{-4} esu^2 cm^2) is the dipole strength via the esu or electrostatic unit, which is a unit of charge in the cgs (centimeter-gram-second) system).

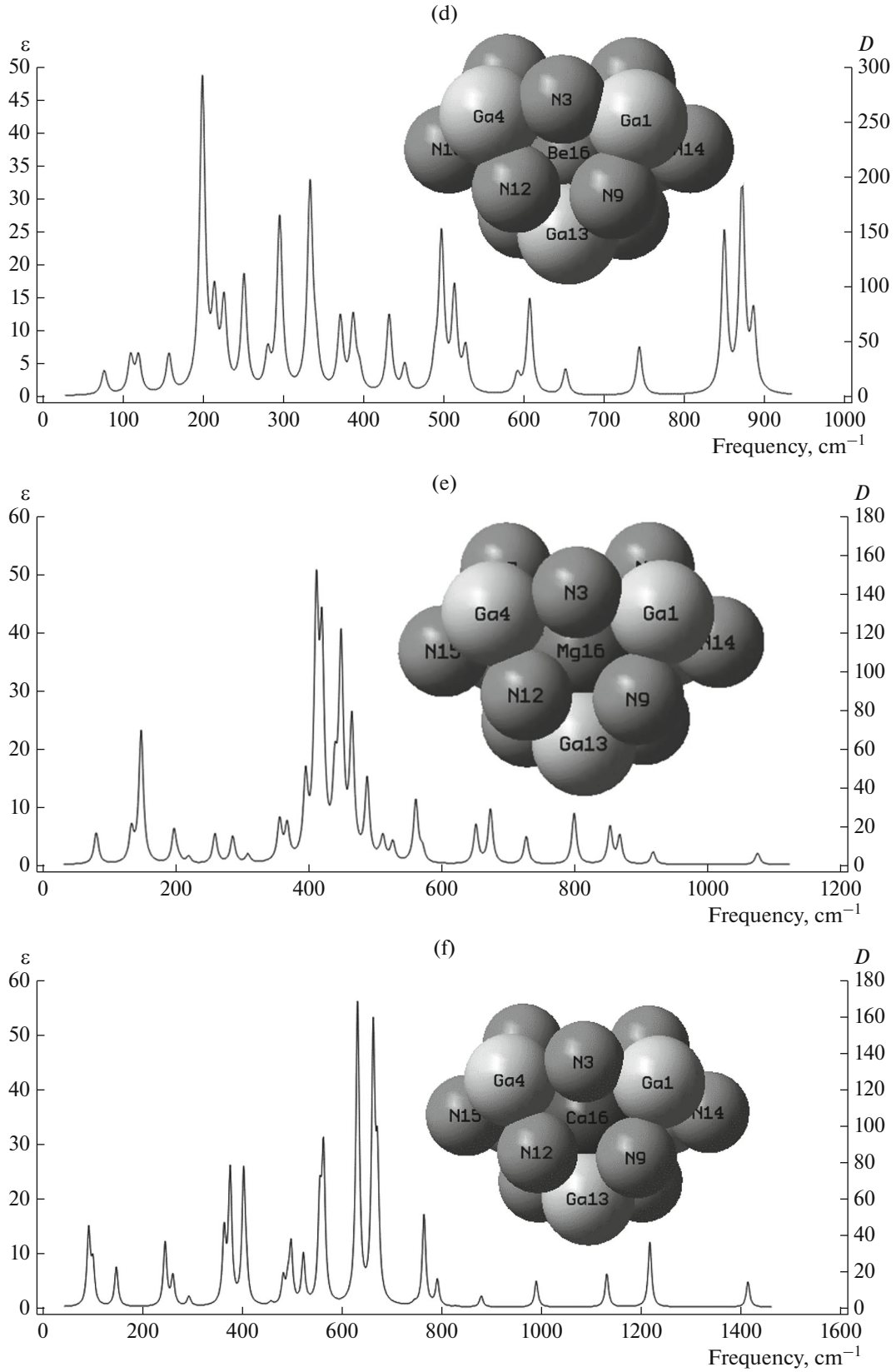
(d)
ε
D
N3
Ga4
Ga1
Be16
N12
N9
Ga13
Frequency, cm−1
(e)
ε
D
N3
Ga4
Ga1
N15
Mg16
N12
N9
Ga13
Frequency, cm−1
(f)
ε
D
N3
Ga4
Ga1
N15
Ca16
N12
N9
Ga13
Frequency, cm−1

Fig. 5. (Contd.)

Table 3. The thermodynamic characters of Li^+@Ga–N, Na^+@Ga–N, K^+@Ga–N, Be^{2+}@Ga–N, Mg^{2+}@Ga–N, and Ca^{2+}@Ga–N complexes using CAM-B3LYP/6-311+G (d,p), LANL2DZ calculation

Compound	$\Delta E^o \times 10^{-4}$, kcal/mol	$\Delta H^o \times 10^{-4}$, kcal/mol	$\Delta G^o \times 10^{-4}$, kcal/mol	S^o, cal/K mol	Dipole moment, Debye
Li^+@Ga–N	–631.1534	–631.1534	–631.1567	112.585	0.2204
Na^+@Ga–N	–640.7248	–640.7247	–640.7280	110.521	0.3167
K^+@Ga–N	–667.8748	–667.8748	–667.8777	99.927	0.5338
Be^{2+}@Ga–N	–631.6031	–631.6030	–631.6065	116.692	0.5200
Mg^{2+}@Ga–N	–643.0713	–643.0712	–643.0745	112.047	0.2905
Ca^{2+}@Ga–N	–672.7063	–672.7062	–672.7093	105.224	0.2896

$$\Delta G_f^o = \Delta G^o_{\mathrm{MC@Ga-N}} - \left(\Delta G^o_{\mathrm{MC-trapped}} + \Delta G^{\mathrm{o}}_{\mathrm{Ga-N}}\right), \quad \mathrm{MC} = \mathrm{Li}^+, \mathrm{Na}^+, \mathrm{K}^+, \mathrm{Be}^{2+}, \mathrm{Mg}^+, \mathrm{Ca}^{2+}. \tag{4}$$

As seen in Table 3, all the accounted ΔG_f^o amounts are very close, which demonstrate the agreement of the measured specifications by all methodologies and the reliability of the computing values.

Table 3 has shown that the dependence on the size of the ions of during interaction between the adsorbates of the alkali and alkaline earth metals cations as the electron acceptors and the adsorbent of Ga–N as electron donor in the complexes of Li^+@Ga–N, Na^+@Ga–N, K^+@Ga–N, Be^{2+}@Ga–N, Mg^{2+}@Ga–N, and Ca^{2+}@Ga–N. Therefore, the selectivity of metal ion by gallium nitride nanocage (ion sensor) can be resulted as: $K^+ > Na^+ > Li^+$ in alkali metals and $Ca^{2+} > Mg^{2+} > Be^{2+}$ in alkaline earth metals.

Recently, Tran and his co-workers have investigated different operational conditions which have been evaluated under batch adsorption experiments, such as pH, NaCl, solid/liquid ratio, stirring speed, contact time, solution temperature, initial adsorbate concentration [59]. The reusability of laden materials was measured through adsorption–desorption cycles. Adsorption kinetics, isotherm, thermodynamics, and mechanisms are studied and discussed. Machine learning processes and statistical physics models are also applied in the field of adsorption science and technology [60, 61].

The binding energy (BE) N–Ga has been evaluated at 398.1 eV. Our results suggest a strong correlation between the electronic and chemical properties of the gallium nitride nanocage. Moreover, it was assigned a feature of BE at 529.69 eV for O–Ga, which most likely formed as the result of a Ga-terminated surface structure.

4. CONCLUSIONS

Ion separation involving a gallium nitride (Ga–N) nanocage can be used to remove a series of alkali and alkaline earth metals cations from aqueous solutions based on electrostatic interactions between the metal cations and Ga–N.

The electromagnetic and thermodynamic properties of alkali/alkaline earth-metal–adsorbed Ga–N system was investigated using density functional theory. The results have illustrated that all the alkali/alkaline earth-metal–adsorbed Ga–N are rather stable with the most stable adsorption site being in the center of Ga–N system. The absorption of alkali/alkaline earth-metal cations in the Ga–N occurs via chemisorption. The *n*-trapping behavior can be found in Ga–N after the adsorption of alkali/alkaline earth-metal cations. The work function of Ga–N has considerably shown the alkali/alkaline earth-metal cation adsorption with maximum amount for the Ca^{2+}/K^+–adsorbed Ga–N system.

ACKNOWLEDGMENTS

In successfully completing this paper and its research, the authors are grateful to Kastamonu University.

FUNDING

This work was supported by ongoing institutional funding. No additional grants to carry out or direct this particular research were obtained.

CONFLICT OF INTEREST

The authors of this work declare that they have no conflicts of interest.

REFERENCES

1. A. H. Davtyan, Z. O. Manukyan, S.D. Arsentev, et al., Russ. J. Phys. Chem. B **17**, 336–345 (2023). https://doi.org/10.1134/S1990793123020239
2. M. Monajjemi, F. Mollaamin, M.R. Gholami, et al., Main Group Met. Chem. **26**, 349 (2003). https://doi.org/10.1515/MGMC.2003.26.6.349
3. G. V. Simbirtseva, S. D. Babenko, D. P. Kiryukhin, et al., Russ. J. Phys. Chem. B **17**, 107–112 (2023). https://doi.org/10.1134/S1990793123010116
4. F. Mollaamin and M. Monajjemi, J. Mol. Model. **29**, 119 (2023). https://doi.org/10.1007/s00894-023-05526-3
5. M. Khaleghian, M. Zahmatkesh, F. Mollaamin, et al., Fuller. Nanotub. Carbon Nanostruct. **19**, 251–261 (2011). https://doi.org/10.1080/15363831003721757
6. F. Esmaeilion, Appl. Water Sci. **10**, 84 (2020). https://doi.org/10.1007/s13201-020-1168-5
7. F. Mollaamin and M. Monajjemi, Russ. J. Phys. Chem. **97**, 2241 (2023). https://doi.org/10.1134/S0036024423100096
8. M. Monajjemi, F. Mollaamin, and S. Shojaei, Biointerface Res. Appl. Chem. **10**, 5575 (2020). https://doi.org/10.33263/BRIAC103.575585
9. F. Mollaamin and M. Monajjemi, Mol. Simul. **49**, 365 (2023). https://doi.org/10.1080/08927022.2022.2159996
10. A. E. Lazhko, M. O. Kostenko, E. A. Lagunova, et al., Russ. J. Phys. Chem. B **16**, 1253–1258 (2022). https://doi.org/10.1134/S1990793122070119
11. M. Monajjemi, M. Noei, and F. Mollaamin, Nucleos. Nucleot. Nucl. **29**, 676–683 (2010). https://doi.org/10.1080/15257771003781642
12. N. V. Dokhlikova, A. K. Gatin, S. Y. Sarvadiy, et al., Russ. J. Phys. Chem. B **16**, 772–779 (2022). https://doi.org/10.1134/S1990793122040042
13. F. Mollaamin and M. Monajjemi, Sensor Review **43**, 266–279 (2023). https://doi.org/10.1108/SR-03-2023-0040
14. M. Monajjemi, M. T. Baie, and F. Mollaamin, Russ. Chem. Bull. **59**, 886–889 (2010). https://doi.org/10.1007/s11172-010-0181-5
15. P. R. Vasyutin, Y. A. Gordienko, M. Y. Sinev, et al., Russ. J. Phys. Chem. B **16**, 1259–1266 (2022). https://doi.org/10.1134/S199079312207017X
16. T. Bhattacharjee, H. Jiang, and N. Behdad, IEEE Sens. J. **15**, 819–826 (2015). https://doi.org/10.1109/JSEN.2014.2351813
17. A. T. Batayneh, Int. J. Environ. Sci. Technol. **9**, 153–162 (2012). https://doi.org/10.1007/s13762-011-0009-3
18. R. Alaya, K. Kourchid, Y. Althaqafi, et al., Russ. J. Phys. Chem. B **17**, 868–877 (2023). https://doi.org/10.1134/S1990793123040024
19. M. Zenk, G. Lukin, D. Bastin, et al., Crystals **12**, 1248 (2022). https://doi.org/10.3390/cryst12091248
20. B. Y. Li, M. Wang, Russ. J. Phys. Chem. B **17**, 878–885 (2023). https://doi.org/10.1134/S1990793123040103
21. P. Mazur, A. Sabik, R. Lewandków, et al., Crystals **12**, 1847 (2022). https://doi.org/10.3390/cryst12121847
22. F. Mollaamin and M. Monajjemi, J. Mol. Model. **29**, 170 (2023). https://doi.org/10.1007/s00894-023-05567-8
23. N. A. Kochetov, Russ. J. Phys. Chem. B **16**, 621–628 (2022). https://doi.org/10.1134/S1990793122040078
24. H. Wang, Z. Xie, Z. Zhou, et al., Russ. J. Phys. Chem. B **15**, 949–953 (2021). https://doi.org/10.1134/S1990793121060269
25. X. Miao, S. Zhou, and C. Wang, Russ. J. Phys. Chem. B **16**, 804–808 (2022). https://doi.org/10.1134/S199079312204011X
26. M.-H. Chen, J.-Y. Li, and V.-C. Su, Crystals **11**, 1320 (2021). https://doi.org/10.3390/cryst11111320
27. M. G. Kucherenko, P. P. Neyasov, and Kruchinin, N. Y. Russ. J. Phys. Chem. B **17**, 745–754 (2023). https://doi.org/10.1134/S1990793123030053
28. B. Esfandiari, F. Mollaamin, M. Monajjemi, M. et al., Russ. J. Phys. Chem. B **17**, 1069–1082 (2023). https://doi.org/10.1134/S1990793123050196
29. S. Bagheri, M. Monajjemi, A. Ziglari, et al., Russ. J. Phys. Chem. B **15** (Suppl. 1), S140–S148 (2021). https://doi.org/10.1134/S1990793121090049
30. M. Monajjemi, M. Khaleghian, N. Tadayonpour, et al., Int. J. Nanosci. **9**, 517–529 (2010). https://doi.org/10.1142/S0219581X10007071
31. H. Touhami, K. Almi, S. Lakel, et al., Russ. J. Phys. Chem. B **17**, 1057–1068 (2023). https://doi.org/10.1134/S1990793123050287
32. R. R. Kayumov, A. P. Radaeva, A. A. Krupina, et al. Russ. J. Phys. Chem. B **17**, 801–809 (2023). https://doi.org/10.1134/S1990793123040097
33. F. Mollaamin, M. Monajjemi, Computation **11**, 108 (2023). https://doi.org/10.3390/computation11060108
34. E. A. Neskoromnaya, A. V. Babkin, E. A. Zakharchenko, et al., Russ. J. Phys. Chem. B **17**, 818–825 (2023). https://doi.org/10.1134/S1990793123040139
35. F. Mollaamin and M. Monajjemi, Russ. J. Phys. Chem. B **17**, 658 (2023). https://doi.org/10.1134/S1990793123030223
36. E. I. Rudenko, N. V. Dohlikova, A. K. Gatin, et al., Russ. J. Phys. Chem. B **17**, 845–852 (2023). https://doi.org/10.1134/S1990793123040164
37. F. Mollaamin, S. Shahriari, M. Monajjemi, et al., J. Clust. Sci. **34**, 1547–1562 (2023). https://doi.org/10.1007/s10876-022-02335-1

38. V. L. Bodneva, M. A. Kozhushner, B. V. Lidskii, et al., Russ. J. Phys. Chem. B **17**, 783–789 (2023). https://doi.org/10.1134/S1990793123040048
39. F. Mollaamin and M. Monajjemi, J. Clust. Sci. **34**, 2901 (2023). https://doi.org/10.1007/s10876-023-02436-5
40. B. Khalili Hadad, F. Mollaamin, and M. Monajjemi, Russ. Chem. Bull. **60**, 238–241 (2011). https://doi.org/10.1007/s11172-011-0039-5
41. F. Mollaamin and M. Monajjemi, J. Bio. Tribo. Corros. **9**, 33 (2023). https://doi.org/10.1007/s40735-023-00751-y
42. M. R. Sarvestani, Z. Doroudi, Russ. J. Phys. Chem. B **16**, 820–826 (2022). https://doi.org/10.1134/S1990793122050098
43. F. Mollaamin, A. Ilkhani, N.Sakhaei, et al., J. Comput. Theor. Nanosci. **12**, 3148–3154 (2015). https://doi.org/10.1166/jctn.2015.4092
44. L. A. Savintseva, A. A. Avdoshin, and S. K. Ignatov, Russ. J. Phys. Chem. B **16**, 445–454 (2022). https://doi.org/10.1134/S1990793122030216
45. P. Hohenberg and W. Kohn, Phys. Rev. B **136**, B864–B871 (1964). https://doi.org/10.1103/PhysRev.136.B864
46. W. Kohn and L. J. Sham, Phys. Rev. **140**, A1133–A1138 (1965). https://doi.org/10.1103/PhysRev.140.A1133
47. A. D. Becke, J. Chem. Phys. **9**, 5648–5652 (1993). https://doi.org/10.1063/1.464913
48. C. Lee, W. Yang, and R. G. Parr, Phys. Rev. B **37**, 785–789 (1988). https://doi.org/10.1103/PhysRevB.37.785
49. Zy. Chen and Jl. Yang, Front. Phys. China **1**, 339–343 (2006). https://doi.org/10.1007/s11467-006-0026-8
50. T. Yanai, D. P. Tew, and N. C. Handy, Chem. Phys. Lett. **393**, 51–57 (2004). https://doi.org/10.1016/j.cplett.2004.06.011
51. M. P. Bircher, and U. Rothlisberger, J. Chem. Theory Comput. **14**, 3184–3195 (2018). https://doi.org/10.1021/acs.jctc.8b00069
52. M. J. Frisch, G. W. Trucks, H. B. Schlegel, G. E. Scuseria, M. A. Robb, J. R. Cheeseman, G. Scalmani, V. Barone, G. A. Petersson, H. Nakatsuji, X. Li, M. Caricato, A. V. Marenich, J. Bloino, B. G. Janesko, R. Gomperts, B. Mennucci, H. P. Hratchian, J. V. Ortiz, A. F. Izmaylov, J. L. Sonnenberg, D. Williams-Young, F. Ding, F. Lipparini, F. Egidi, J. Goings, B. Peng, A. Petrone, T. Henderson, D. Ranasinghe, V. G. Zakrzewski, J. Gao, N. Rega, G. Zheng, W. Liang, M. Hada, M. Ehara, K. Toyota, R. Fukuda, J. Hasegawa, M. Ishida, T. Nakajima, Y. Honda, O. Kitao, H. Nakai, T. Vreven, K. Throssell, J. A. Montgomery, Jr., J. E. Peralta, F. Ogliaro, M. J. Bearpark, J. J. Heyd, E. N. Brothers, K. N. Kudin, V. N. Staroverov, T. A. Keith, R. Kobayashi, J. Normand, K. Raghavachari, A. P. Rendell, J. C. Burant, S. S. Iyengar, J. Tomasi, M. Cossi, J. M. Millam, M. Klene, C. Adamo, R. Cammi, J. W. Ochterski, R. L. Martin, K. Morokuma, O. Farkas, J. B. Foresman, and D. J. Fox, *Gaussian 16, Revision C.01* (Gaussian, Inc., Wallingford CT, 2016).
53. R. Dennington, T. A. Keith, and J. M. Millam, *GaussView, Version 6.06.16* (Semichem Inc., Shawnee Mission, KS, 2016).
54. J. Smith, Nature **270**, 663 (1977). https://doi.org/10.1038/270663a0
55. K. Bakhshi, F. Mollaamin, M. Monajjemi, J. Comput. Theor. Nanosci. **8**, 763–768 (2011). https://doi.org/10.1166/jctn.2011.1750
56. M. A. A. Zadeh, H. Lari, L. Kharghanian, et al., J. Comput. Theor. Nanosci. **12**, 4358 (2015). https://doi.org/10.1166/jctn.2015.4366
57. H. A. Young and R. D. Freedman, *Sears and Zemansky's University Physics with Modern Physics*, 13th ed. (Addison-Wesley, Boston, 2012), p. 754.
58. F. Mollaamin, M. Monajjemi, S. Salemi, et al., Fuller. Nanotub. Carbon Nanostruct. **19**, 182 (2011). https://doi.org/10.1080/15363831003782932
59. H. N. Tran, Water **15**, 2857 (2023). https://doi.org/10.3390/w15152857
60. N. V. Dokhlikova, S. A. Ozerin, S. V. Doronin, et al., Russ. J. Phys. Chem. B **16**, 461–467 (2022). https://doi.org/10.1134/S1990793122030137
61. A. V. Fedotov, A. A. Svittsov, and V. I. Vanchurin, Russ. J. Phys. Chem. B **15**, 1200–1206 (2021). https://doi.org/10.1134/S1990793121070046